Detour phase Talbot array illuminator

Zhigang Li (李志刚)[1], Rui Yang (杨 瑞)[1], Meiyu Sun (孙美玉)[1], Jing Han (韩 靖)[1], Dengying Zhang (张登英)[1], Jiannong Chen (陈建农)[1], Dawei Zhang (张大伟)[2], and Linwei Zhu (朱林伟)[1,*]

[1]*School of Physics and Optoelectronic Engineering, Ludong University, Yantai 264025, China*
[2]*Engineering Research Center of Optical Instrument and System, Ministry of Education, Shanghai Key Laboratory of Modern Optical System, School of Optical-Electrical and Computer Engineering, University of Shanghai for Science and Technology, Shanghai 200093, China*
**Corresponding author: lwzhu@siom.ac.cn*

Received January 10, 2019; accepted March 22, 2019; posted online June 6, 2019

In this Letter, we propose a simple and effective approach for transforming a conventional Talbot array illuminator (TAI) with multilevel phase steps into a binary-phase TAI (BP-TAI) through detour phase encoding. The BP-TAI is a binary ($0\ \pi$) phase-only diffractive optical element, which can be utilized to generate a large-scale focal spots array with a high compression ratio. As an example, we design a square BP-TAI with the fraction parameter $\beta = 15$ for achieving a square multifocal lattice with a high compression ratio β^2. Theoretical analysis and experimental results demonstrate that the detour phase encoding is efficient for designing the BP-TAI, especially with the high compression ratio. Such results may be exploited in practical large-scale optical trapping and X-ray imaging.

OCIS codes: 050.1950, 070.6760, 050.1380.
doi: 10.3788/COL201917.070501.

The fractional Talbot effect is an interesting diffractive phenomenon where an input object wave with a periodic distribution generates a phase-only pattern at the fractional Talbot distance and vice versa[1]. Hence, the Talbot array illuminator (TAI) can be realized when the phase-only distribution of the periodic object is established at the fractional Talbot distance[2]. The TAI is a phase-only diffractive element that can transform a plane wave into a large-scale optical array of bright spots with high efficiency and high compression ratio. The compression ratio signifies the focusing capacity of the TAI, which can be defined approximately as the ratio of the area of an incident beam to the area of the bright spots in the fractional plane. It has been demonstrated that the TAI can be applied in constructing large-scale optical traps on a chip for optical sorting[3–6], high-accuracy measurement, wavefront sensing[7–10], multiple imaging[11–13], multiple duplication lithography, and Talbot interference lithography[14–17]. To obtain a high compression ratio phase-only TAI for enhancing the intensity of the output array spots, the conventional TAI must be fabricated into a multilevel phase element[18–20]. However, it is tough to achieve such multilevel phase elements by using the frequently used laser direct writing device or the ion etching equipment. Even though the multilevel TAI can be realized using other techniques, the manufacturing processes are time-consuming and costly, and the accuracy is also not high, which severely limits its application in practice. Thus, how to transform the multilevel phase of a conventional TAI into a binary ($0\ \pi$) one with a high compression ratio has become an urgently needed challenge to achieve.

In this Letter, we proposed a novel method for achieving a binary-phase ($0\ \pi$) TAI (BP-TAI) with a high compression ratio based on detour phase encoding (DPE). In our previous work[21], we have accomplished some simple analytical equations for calculating the phase-only distribution at any fractional Talbot distance. Based on these formulas, the multilevel phase-only distribution of a conventional TAI with high efficiency and an arbitrary high compression ratio can be designed. For a square array as an example, the unit cell must be a square with a constant amplitude distribution to satisfy the condition of connecting the adjacent spots, which is the necessary prerequisite for attaining the phase-only TAI with high efficiency[22]. The phase of each unit cell at the position of the square array point (m, n) can be established by the following formula:

$$\varphi(m,n,\beta) = \begin{cases} (1-1/\beta)(m^2+n^2)\pi, & \beta = 4L-2 \\ (-1/\beta)(m^2+n^2)\pi, & \beta = 4L \\ (-1-1/\beta)(m^2+n^2)\pi/2, & \beta = 4L-1 \\ (1-1/\beta)(m^2+n^2)\pi/2, & \beta = 4L+1 \end{cases}, \tag{1}$$

where m and n are the position numbers of the unit cells in the square array; β is an integer, known as the fraction parameter, which also determines the phase levels l and the compression ratio γ of the TAI; L is a positive integer, which limits the values of the fraction parameter β. There are four cases of phase distribution, depending on the values of the fraction parameter β, as shown in Eq. (1).

According to our previous discussion[21], the phase-only distribution of the TAI is a periodic structure. The phase of the unit cell repeats periodically in the two directions of the square. Thus, the whole phase distribution of the

TAI can be obtained through the phase distribution in only one period. Based on the phase analytical equation shown in Eq. (1), the phase-only distribution pattern in one period can be written as

$$u(x,y) = \mathrm{rect}\left(\frac{x}{w},\frac{y}{w}\right) \times \left\{ u_0(x,y) \otimes \sum_{m=0}^{\beta-1}\sum_{n=0}^{\beta-1} \delta(x-m\Delta, y-n\Delta)\exp[i\varphi(m,n,\beta)] \right\}, \quad (2)$$

where $u_0 = \mathrm{rect}(x/\Delta, y/\Delta)$ is the rectangle function with the width Δ, giving the size of the unit cell; the rectangle function $\mathrm{rect}(x/w, y/w)$ with the width of $w = \beta\Delta$ indicates the size of the periodic unit [marked in Fig. 1(c) when $\beta = 15$] of the square array. The symbol $\otimes$ denotes convolution operation. As shown in Eq. (2), the numbers of unit cells in one periodic unit are $\beta \times \beta$. Then, the phase-only distribution of the square TAI can be expressed as

$$U(x,y) = u(x,y) \otimes \sum_{M_0=1}^{M}\sum_{N_0=1}^{N} \delta(x - M_0 w, y - N_0 w), \quad (3)$$

where M_0 and N_0 are the period numbers of the square array along the x and y directions, respectively. M and N are the maximum period numbers. Then, a square multifocal spots array with compression ratio $\gamma = \beta^2$ can be created at the corresponding fractional distance when the TAI is illuminated by a coherent plane wave. It should be noted that the fractional Talbot distance with the phase distribution of Eq. (1) is given by $z = \beta\Delta^2/\lambda$ when β is an odd number, while $z = 2\beta\Delta^2/\lambda$ when β is an even number, where λ is the wavelength of the illumination beam.

Figure 1 gives an example of a square TAI with fraction parameter $\beta = 15$ and period numbers $M = N = 6$.

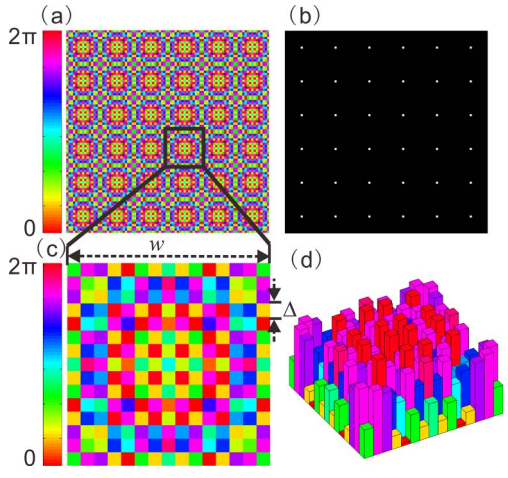

Fig. 1. (a) Example of conventional TAI for a square array designed according to Eq. (1) with a fraction parameter of $\beta = 15$, and (b) its reconstructed intensity distribution at the fractional distance. (c) Phase distribution within one period of the TAI and (d) its corresponding 3D multilevel steps structure.

The size of the unit cell is $\Delta = 60$ μm, and the wavelength of the incident light is 532 nm. Figure 1(a) shows the phase distribution of the TAI calculated by Eq. (1). Figure 1(b) shows the diffractive intensity distribution at the corresponding fractional Talbot distance of $z = 101.5$ mm. It is clear that the TAI with the phase-only distribution shown in Fig. 1(a) can successfully transform the input plane beam into a 6×6 multifocal square array with the high compression ratio $\gamma = 225$.

However, the TAI with high compression ratio is a multilevel phase-only optical element. Figure 1(c) shows the phase distribution within one period. Figure 1(d) is the corresponding three-dimensional (3D) steps structure. We can see that the phase distribution of the TAI has a complex multilevel structure. For designing a TAI with an arbitrary compression ratio using the phase-only analytical expression of Eq. (1), the phase level of the TAI is equal to the fraction parameter, that is $l = \beta$. Figure 2 shows the stem plot of the phase distribution of the TAI within one period with $\beta = 15$ [as shown in Fig. 1(c)]. It is shown that the phase level is equal to the fraction parameter β, which means the TAI must be fabricated into fifteen relief steps in different array positions. While the TAI has a higher compression ratio, the phase structure of the TAI will become more complex. Hence, it is unattainable to fabricate such a high compression ratio TAI using the traditional laser direct writing device or the ion etching equipment. However, the difficulty of achieving multilevel phase TAI will be resolved when the multilevel phase can be transformed into a binary $(0\ \pi)$ phase. That is because the fabrication of the binary phase-only element is relatively straightforward. Furthermore, the binary diffraction element can also be duplicated easily.

The DPE method has been widely utilized in the computer-generated hologram (CGH)[23]. The hologram generated by using the Lohmann DPE is a binary element[24–26]. Therefore, we can transform the multilevel phase distribution into a binary structure using Lohmann DPE. The core technology of the Lohmann DPE is to control the amplitude by modulating the size of an aperture within each cell and to control the phase by modulating the lateral positions of the aperture proportioned to the transform phase at the center of its cell.

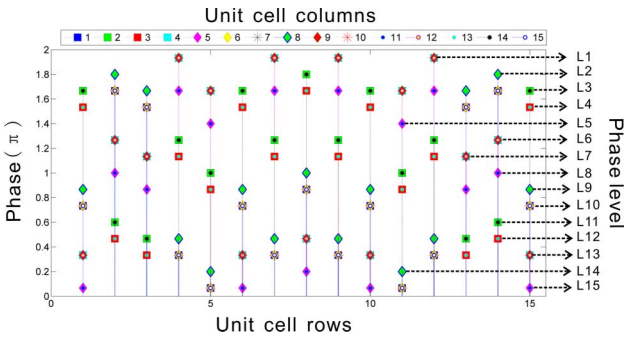

Fig. 2. Stemplot of the phase levels as shown in Fig. 1(c).

Similarly, for a conventional phase-only TAI, the invariable amplitude of the TAI can be encoded through a rectangular aperture with a half-width of the unit cell [as shown in Fig. 3(a)], while the lateral displacement between the center of the unit cell and the center of the rectangular aperture is used for encoding the phase. Hence, for designing the BP-TAI, we just need to precisely manipulate the lateral position of each unit cell in the TAI. Based on the theory of the DPE method, the lateral displacement of the BP-TAI can be written as

$$\delta_{mn} = \frac{\varphi(m, n, \beta)}{2\pi}\Delta, \tag{4}$$

where δ_{mn} is the lateral displacement at the position of the (m, n) array point, and Δ is the size of the unit cell. Equation (4) shows that the lateral displacement is proportional to the phase of the transform $\varphi(m, n, \beta)$, which is given in Eq. (1). Moreover, it should be noted that the range of the phase values in Eq. (4) is limited to $[0, 2\pi]$. An essential part of the BP-TAI is to establish the lateral displacement of each cell. Thus, once the geometrical structure of the BP-TAI is constructed, it will be easy to fabricate and reproduce the array elements with high compression ratio, because the BP-TAI has only a two-step phase [as shown in Fig. 3(b)]. In that case, the function of the converted unit cell with shifting aperture can be expressed as

$$u_{mn}(x, y) = u_0(x, y) - 2 \times \mathrm{rect}\left(\frac{x - \delta_{mn}}{\Delta/2}, \frac{y}{\Delta}\right), \tag{5}$$

where u_{mn} is the function of the unit cell at the position of (m, n). Then, the function of the square array in one period can be rewritten as

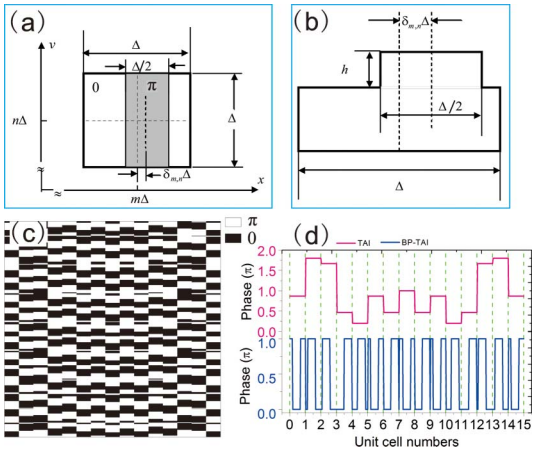

Fig. 3. (a) Structure of the (m, n) cell in the BP-TAI and (b) its phase configuration. The rectangular opening has a width $\Delta/2$ and a height h, and it is shifted from the center of the cell at $(m\Delta, n\Delta)$ by $\delta_{mn}\Delta$. (c) Phase distribution within one period of the BP-TAI with $\beta = 15$. (d) Comparison diagram of the phase distributions along the line through the center of the BP-TAI and the conventional TAI with $\beta = 15$.

$$u(x,y)=\mathrm{rect}\left(\frac{x}{w},\frac{y}{w}\right)\times\left[\sum_{m=0}^{\beta-1}\sum_{n=0}^{\beta-1}u_{mn}(x,y)\otimes\delta(x-m\Delta,y-n\Delta)\right]. \tag{6}$$

According to Eq. (6), the phase distribution in one period of the BP-TAI can be established. Figure 3(c) shows the phase distribution of the BP-TAI in one period with $\beta = 15$. It is shown that the BP-TAI is composed of different rectangles of sizes and positions, but the phase distribution has only two values, 0 and π. Figure 3(d) shows the comparison diagram of phase distributions between the BP-TAI and the conventional TAI along the line through the center of the two types of array illuminators with $\beta = 15$. It is clear that the multilevel phase-only TAI has been transformed into a binary-phase element. Based on the Lohmann DPE, the phase distribution of the multilevel TAI with high compression ratio has been changed from the original unit cell with uniform size and different multilevel phase into a new cell with binary phase and different lateral displacement. It should be noted that the design parameters in Eqs. (4) and (5) are selected to avoid the reconstructed noise and realize a high diffraction efficiency. Generally, in order to achieve high diffraction efficiency, the diffraction image of the detour phase is selected at the first diffraction order. The geometrical shape of the shifting slit shown in Fig. 3(a) is chosen to achieve a high diffraction efficiency using a proper width and position. In addition, phase errors caused by deviations in the etching depths during the lithographic fabrication will also affect the diffraction efficiency of the element.

Based on the binary-phase distribution in one period of the BP-TAI, we can realize a square multifocal array with a high compression ratio. We evaluate the proposed approach using the experimental setup shown in Fig. 4(a). In this setup, we use laser light with a wavelength of 532 nm for incident light (LWGL532, Beijing Laserwave Optoelectronics Technology Co., Ltd., China). A CCD (EO-5012, Edmund Optics, US) is used to record the image of the multifocal spots array diffracted from the

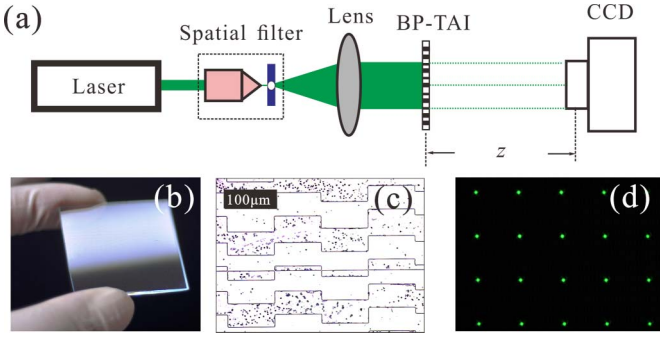

Fig. 4. (a) Experimental setup for evaluation. (b) Photo of the BP-TAI fabricated using the binary-phase distribution shown in Fig. 3(c). (c) The microscopy image of the BP-TAI. (d) Experimental results of intensity distribution at the corresponding fractional Talbot distance of the BP-TAI.

BP-TAI. The distance between the BP-TAI and the CCD is equal to the fractional Talbot distance $z = \beta\Delta^2/\lambda$. Figure 4(b) shows the real photo of the BP-TAI, which is fabricated by using the wet etching technology with the illuminating wavelength of $\lambda = 532$ nm. Figure 4(c) shows the microscopy imaging of the BP-TAI, in which the minimum line-width is 3 μm, the width of the unit cell is $\Delta = 90$ μm, and the fraction parameter is $\beta = 15$. This type of BP-TAI can be used for generating a 40×40 square array spot with a high compression ratio of $\gamma = 225$. Figure 4(d) shows the diffractive intensity distribution at the corresponding fractional Talbot distance of $z = \beta\Delta^2/\lambda = 228.4$ mm. It is clear that the BP-TAI coded by Lohmann DPE successfully transforms the input plane beam into a square multifocal array with a high compression ratio. Consequently, the DPE method is a highly effective approach for transformation of the multilevel phase-only TAI into a binary phase-only element.

In the experiment, the laser power of the square array spots and the incident beam can be obtained. Using the two parameters, the diffraction efficiency of the BP-TAI can be calculated approximately. The efficiency of the BP-TAI used in the experiment is about 40%. The fabrication errors and other diffraction orders resulting from DPE cause the loss of diffraction efficiency and quality of the reconstruction image. Figures 5(a) and 5(b) are the enlarged intensity distribution of one spot diffracted from the BP-TAI in the experimental and simulated results, respectively. Figure 5(c) shows the ideal reconstructed image of one unit cell within the original array object. We can see that the intensity distribution of the spots reconstructed by the BP-TAI is not an ideal square-shaped structure. This is due to the diffraction effect of a limited aperture of the array element, but this edge diffraction effect can be diminished by increasing the size of the diffraction element or the number of the unit cell. Besides, the reconstructed array spots of the BP-TAI can also be affected by other diffraction orders that result from DPE. In order to avoid the effect caused by the other diffraction orders, the diffraction angle of the BP-TAI should be designed to be as large as possible. Figure 5(d) shows a comparison of cross-sections of the intensity distribution within one period of the spots array (note the logarithmic scale). It is shown that the noise of the output array reconstructed by the BP-TAI is about 1% when $\beta = 15$. However, for the BP-TAI with a high compression ratio, the noise caused by other diffraction orders can be ignored.

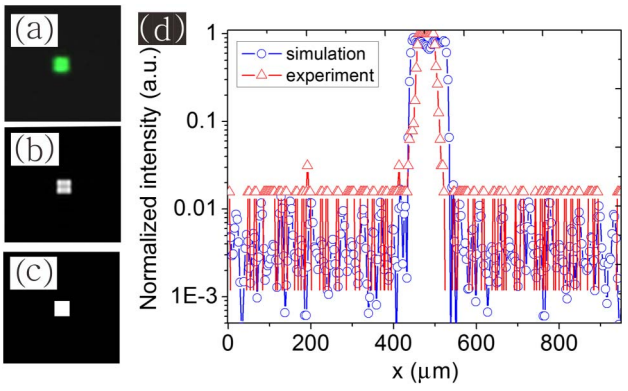

Fig. 5. Intensity distribution of the single focal spot field within one period of the BP-TAI: (a) experiment, (b) simulation, (c) ideal image. (d) Comparison of cross-sections through the intensity fields shown in (a) and (b) (note the logarithmic scale).

Figure 6 shows the noise effect as a function of the fraction parameter β. The noise effect is evaluated by the mean square error (MSE) and the peak signal to noise ratio (PSNR) of the intensity field reconstructed by the BP-TAI in comparison with the ideal image distribution in one period of the array spots. It is clearly seen from Fig. 6 that the noise effect decreases faster with the increase of the fraction parameter β. The MSE is less than 0.1%, and the PSNR can reach up to 80 dB, with the fraction parameter of $\beta = 15$. Hence, the noise caused by DPE can be entirely ignored for designing the BP-TAI with a high compression ratio.

In summary, based on DPE, we derived that the conventional TAI with high compression ratio can be transformed into a binary phase-only array illuminator. The theoretical analysis and the simulation results have demonstrated that the BP-TAI is suitable for designing a high compression ratio TAI. The multilevel phase distribution of the conventional TAI with a high compression ratio can be changed into a binary phase-only structure, in which the phase configurations of the unit cell are only two values (0 and π). In comparison with conventional TAIs, the BP-TAIs overcome the limit of the machining difficulty resulting from the multilevel phase distribution of the phase-only illuminators. Likewise, any other spot arrays with various configurations (such as a hexagonal TAI[27]) can also be realized by converting the corresponding phase distribution into a binary structure with different lateral displacements in the design of the BP-TAIs. Therefore, the BP-TAIs could be used to extend the applications in some fields, such as near-field optical array micromanipulation[28], the far-field diffraction region[29], orbital angular momentum multiplexing[30], prime number decomposition[31], and other fields[32].

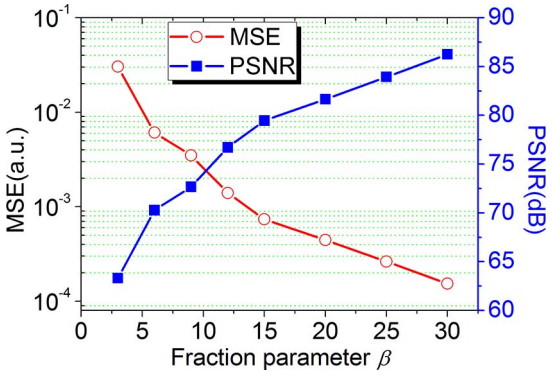

Fig. 6. Noise effect of the BP-TAI versus the fraction parameter.

This work was supported by the National Natural Science Foundation of China (NSFC) (Nos. 61675093 and 61705096), the Natural Science Foundation of Shandong Province (No. ZR2017MA035), the Shandong Province Higher Educational Science and Technology Program (No. J17KA176), and the Taishan Scholars Project of Shandong Province (No. ts2015110055).

References

1. A. W. Lohmann and J. A. Thomas, Appl. Opt. **29**, 4337 (1990).
2. Q. Li, J. Huo, X. Zhao, and X. Chen, Chin. Opt. Lett. **12**, 050701 (2014).
3. G. X. Wei, L. L. Lu, and C. S. Guo, Opt. Commun. **282**, 2665 (2009).
4. C. S. Guo, Y. N. Yu, and Z. P. Hong, Opt. Commun. **283**, 1889 (2010).
5. J. Lamstein, A. Bezryadina, D. Preece, J. C. Chen, and Z. Chen, Chin. Opt. Lett. **15**, 030010 (2017).
6. Z. Liu, T. Wang, Y. Zhang, X. Tang, P. Liu, Y. Zhang, X. Yang, J. Zhang, J. Yang, and L. Yuan, Chin. Opt. Lett. **16**, 053501 (2018).
7. B. Santra, C. Baals, R. Labouvie, A. B. Bhattacherjee, A. Pelster, and H. Ott, Nat. Commun. **8**, 15601 (2017).
8. Y. Liu, M. Seaberg, D. Zhu, J. Krzywinski, F. Seiboth, C. Hardin, D. Cocco, A. Aquila, B. Nagler, H. J. Lee, S. Boutet, Y. Feng, Y. Ding, G. Marcus, and A. Sakdinawat, Optica **5**, 967 (2018).
9. D. Podanchuk, A. Kovalenko, V. Kurashov, M. Kotov, A. Goloborodko, and V. Danko, Appl. Opt. **53**, B223 (2014).
10. D. V. Podanchuk, A. A. Goloborodko, M. M. Kotov, A. V. Kovalenko, V. N. Kurashov, and V. P. Dan'ko, Appl. Opt. **55**, B150 (2016).
11. Y. Zhai, C. H. Carson, V. A. Henderson, P. F. Griffin, E. Riis, and A. S. Arnold, Optica **5**, 80 (2018).
12. C. Y. Lin, W.-T. Lin, H.-H. Chen, J.-M. Wong, V. R. Singh, and Y. Luo, Opt. Lett. **41**, 344 (2016).
13. Z. Zhang, J. Chang, H. Ren, K. Fan, and D. Li, Chin. Opt. Lett. **17**, 011101 (2019).
14. H.-S. Kim, W. Li, S. Danylyuk, W. S. Brocklesby, M. C. Marconi, and L. Juschkin, Opt. Lett. **39**, 6969 (2014).
15. A. Vetter, R. Kirner, D. Opalevs, M. Scholz, P. Leisching, T. Scharf, W. Noell, C. Rockstuhl, and R. Voelkel, Opt. Express **26**, 22218 (2018).
16. W. Li and M. C. Marconi, Opt. Express **23**, 25532 (2015).
17. B. Dai, H. Wang, Q. Xu, Z. Li, C. Tao, and D. Zhang, Chin. Opt. Lett. **16**, 122201 (2018).
18. V. Arrizon and J. Ojedacastaneda, Appl. Opt. **33**, 5925 (1994).
19. S. Zhao, C. H. Zhou, P. Xi, H. S. Wang, and L. R. Liu, J. Opt. Soc. Am. A **18**, 103 (2001).
20. C. H. Zhou, H. S. Wang, S. Zhao, P. Xi, and L. R. Liu, Appl. Opt. **40**, 607 (2001).
21. L. W. Zhu, X. Yi, Z. Hong, and C. S. Guo, J. Opt. Soc. Am. A **25**, 203 (2008).
22. V. Arrizon, E. Lopez-Olazagasti, and A. Serrano-Heredia, Opt. Lett. **21**, 233 (1996).
23. G. Tricoles, Appl. Opt. **26**, 4351 (1987).
24. B. R. Brown and A. W. Lohmann, Appl. Opt. **5**, 967 (1966).
25. A. W. Lohmann and D. P. Paris, Appl. Opt. **6**, 1739 (1967).
26. M. Fujiwara, N. Takada, H. Araki, S. Ikawa, Y. Maeda, H. Niwase, M. Oikawa, T. Kakue, T. Shimobaba, and T. Ito, Chin. Opt. Lett. **16**, 080901 (2018).
27. C. S. Guo, X. Yin, L. W. Zhu, and Z. Hong, Opt. Lett. **32**, 2079 (2007).
28. L. W. Zhu, J. J. Yu, D. W. Zhang, M. Y. Sun, and J. N. Chen, Opt. Express **22**, 9798 (2014).
29. J. Azana and H. G. De Chatellus, Phys. Rev. Lett. **112**, 213902 (2014).
30. J. S. Rodrigues, C. V. C. Mendes, E. J. S. Fonseca, and A. J. Jesus-Silva, Opt. Lett. **42**, 3944 (2017).
31. K. Pelka, J. Graf, T. Mehringer, and J. von Zanthier, Opt. Express **26**, 15009 (2018).
32. J. Wen, Y. Zhang, and M. Xiao, Adv. Opt. Photon. **5**, 83 (2013).